npj | climate and atmospheric science

Article

Published in partnership with CECCR at King Abdulaziz University

https://doi.org/10.1038/s41612-026-01463-z

# Facets of the tropical high-cloud feedback in a global storm-resolving model

Check for updates

Jakob Deutloff[1,2,3] ✉, Stefan A. Buehler[1,2], Julia M. Windmiller[4,5] & Ann Kristin Naumann[6]

Tropical high clouds are the cloud type that contributes most to the uncertainty in climate sensitivity, as their feedback on global warming remains poorly constrained. One reason for this is that global circulation models (GCMs) do not resolve the full spectrum of high clouds, ranging from thin cirrus to thick deep convective clouds. We use a set of storm-resolving aquaplanet simulations that resolve this spectrum to investigate how high clouds with different thicknesses contribute to the total high-cloud feedback. We find that the total feedback is positive, arising from all high clouds remaining at fixed temperatures and from an intensification of the diurnal cycle of deep convection. Fixed high-cloud temperatures require an interactive representation of ozone. Prescribing ozone, as often done in GCMs, results in an unrealistic warming of high clouds and hence a less positive feedback. Thick clouds produced by deep convection partly shift from daytime to nighttime in response to surface warming. This reduces sunlight reflection and results in a previously unrecognised positive feedback. The reduction of high clouds in response to warming, assumed to produce a negative feedback, affects thin (warming) and thick (cooling) clouds equally in our simulations, resulting in a near-neutral feedback.

High clouds fed by deep convection occur throughout the tropics, but remain difficult to predict due to their multiscale nature, spanning from the microscale of individual droplets, through the mesoscale of convective systems, to the synoptic scale of the intertropical convergence zone[1]. As a result, tropical high clouds are the cloud type contributing most to the uncertainty in climate sensitivity, with their feedback on global warming being poorly constrained[2].

Progress in reducing the uncertainty in the response of tropical high clouds to surface warming has been difficult, partly because global circulation models (GCMs) have limited ability to capture the details of tropical convection. With a typical horizontal grid-spacing of $\mathcal{O}(100\,\mathrm{km})$, those models do not resolve convection or individual clouds and hence rely on parameterisations for those processes, which cause vast inter-model differences in the cloud response to warming[3,4].

There is hope that the shortcomings of GCMs for simulating clouds can be overcome by global storm-resolving models (GSRMs) with a horizontal grid-spacing of $\mathcal{O}(1\,\mathrm{km})$[5]. Those models do not depend on parameterisations of convection since it is simulated explicitly, and clouds are resolved in the sense that microphysical models directly respond to grid-scale forcing[6]. GSRMs indeed represent some aspects of the tropical climate more accurately than GCMs: the diurnal cycle and the spatial distribution of precipitation are better captured[7], and the inter-model spread of relative humidity is reduced[8].

Another benefit from GSRMs is that their high resolution allows for better interpretability of the results. By resolving high clouds, GSRMs capture the continuum of high clouds that exists in the real world, ranging from thick deep convective towers to thin cirrus[9]. Therefore, the total high-cloud radiative effect can be decomposed into the high-cloud radiative effect as a function of cloud thickness, measured by ice water path ($I$), and the frequency of each $I$[10,11]. This perspective uncovers how clouds with different thicknesses, governed by different physics, contribute to the high-cloud feedback.

We use this $I$-perspective to investigate the tropical high-cloud feedback in a set of global storm-resolving aquaplanet simulations. We will show that the tropical high-cloud feedback consists of three parts: a positive longwave feedback from high clouds remaining at fixed temperature, a positive shortwave feedback from an intensification of the diurnal cycle of convection and a near-neutral feedback from changes in high-cloud frequency. The total tropical high-cloud feedback we derive is positive, in contrast to the near-neutral estimate reported by the World Climate

[1]Earth System Sciences, Atmospheric Science, University of Hamburg, Hamburg, Germany. [2]Earth and Society Research Hub (ESRAH), Hamburg, Germany. [3]International Max Planck Research School on Earth System Modelling (IMPRS-ESM), Hamburg, Germany. [4]Max Planck Institute for Meteorology, Hamburg, Germany. [5]ARC Centre of Excellence for the Weather of the 21st Century, Monash University, Melbourne, VIC, Australia. [6]Ludwig-Maximilians-Universität in Munich, Munich, Germany. ✉e-mail: jakob.deutloff@uni-hamburg.de

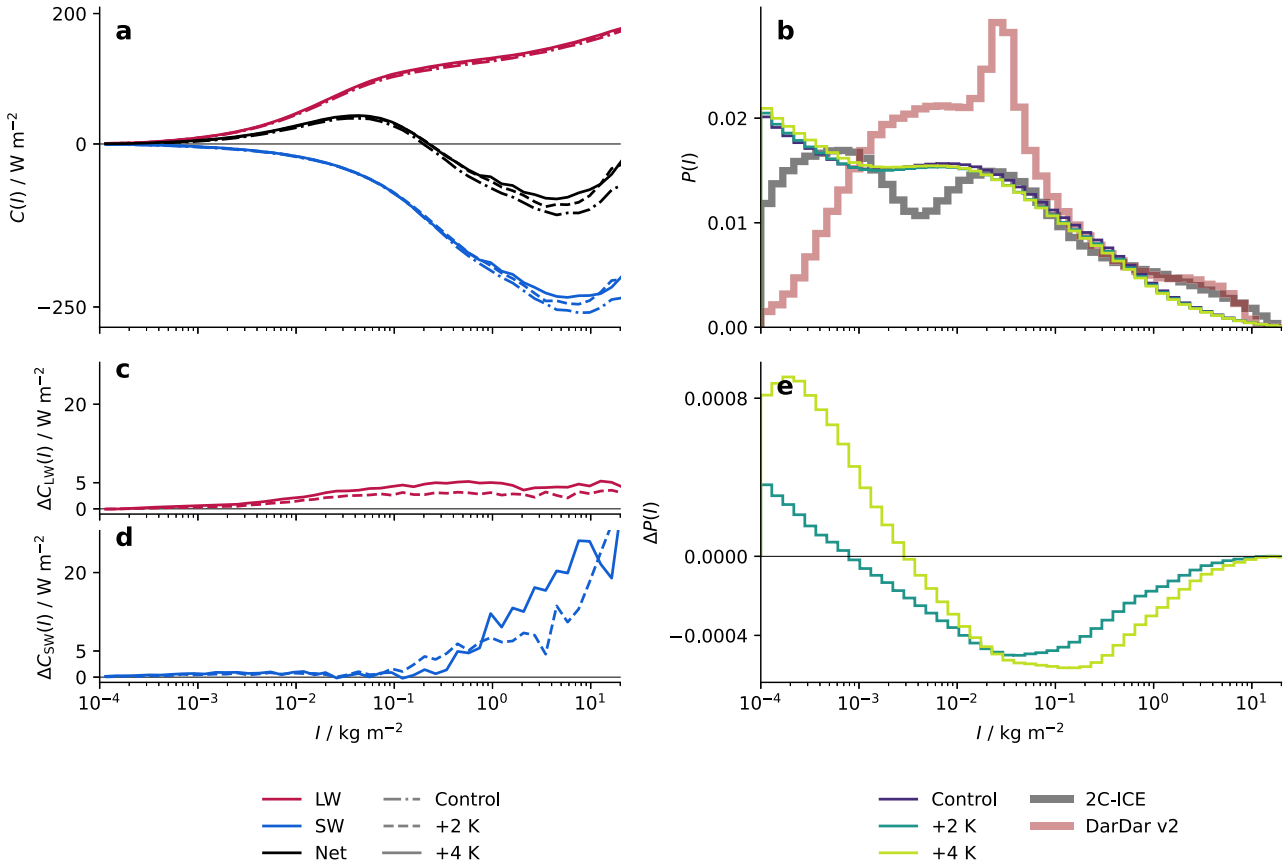



**Fig. 1 | Frequency of tropical high clouds, their radiative effect and how both change in response to surface warming. a** High-cloud radiative effect ($C$) as a function of ice water path ($I$), **b** ice water path frequency distribution ($P$), **c** change of the LW $C$ with respect to the control simulation ($\Delta C_{LW}$), **d** change of the SW $C$ with respect to the control simulation ($\Delta C_{SW}$), **e** change in $P$ with respect to the control simulation ($\Delta P$).

Research Programme (WCRP) expert assessment[2]. This difference arises because the newly identified positive feedback from an intensified diurnal cycle of convection adds to the well-documented[12–14] feedback associated with approximately fixed high-cloud temperatures. In addition, the negative feedback expected by the WCRP assessment from a reduction of tropical high clouds proves to be near-neutral, as both thin (warming) and thick (cooling) clouds decrease with warming. This near-neutral high-cloud amount feedback is in line with recent radiative convective equilibrium (RCE) simulations[11] and observational estimates[15–17].

## Results

### Resolving high clouds at km-scale

We simulate convection explicitly at 5 km horizontal grid spacing with the Sapphire version of the ICOsahedral Nonhydrostatic (ICON) model[18], with parameterised turbulence[19], cloud microphysics[20] and interactive ozone[21]. To allow for short simulation periods while including the main characteristics of tropical convection, we use an aquaplanet setup[22,23] with a prescribed zonally symmetric sea surface temperature (SST) pattern[24] and no seasonal cycle. We conduct a 3-month-long control and two warming simulations with the same simulation period and uniform SST increases of 2 K and 4 K (see 'Methods' for details). Our analysis is constrained to the tropics (20°S to 20°N). By moving to the global scale, including rotation and the diurnal cycle of convection, we go beyond previous, more idealised cloud-resolving model studies[11,25]. Despite their reduced complexity, aquaplanet simulations reproduce key features of the Earth's atmosphere and have proven useful for studying cloud feedbacks [26].

We define high clouds as all clouds that contain frozen condensate. To avoid artificial separation between the frozen and the liquid phase of clouds, we consider liquid condensate to be part of the high cloud if liquid and frozen condensate sufficiently overlap[10] (section 'Methods').

The $I$ frequency distribution, $P(I)$, within the tropics from ICON broadly agrees with satellite retrievals. For $I > 10^{-1}$ kg m$^{-2}$, the ICON simulations agree with both 2C-ICE R05[27] and DARDAR v2.1.1[28] that high clouds become more frequent the thinner they are (Fig. 1b). However, deep convective clouds with $I > 1$ kg m$^{-2}$ are approximately half as frequent in ICON as in both 2C-ICE and DARADAR. This is a common bias of GSRMs[9], which might stem from unrealistic parameterisations of cloud microphysics and too coarse grid spacing. Simulations with improved parameterisations of cloud microphysics and a horizontal grid spacing of 1 km yield a deep convective cloud amount that agrees well with observations[29]. Differences between ICON and the satellite retrievals for $I < 10^{-1}$ kg m$^{-2}$ are significant, but should not be overinterpreted as the two retrievals also do not agree in this domain.

The high-cloud radiative effect, $C(I)$, calculated from the ICON simulations exhibits the characteristic shape[11,30] of a positive net $C(I)$ for small $I$ and a negative net $C(I)$ for high $I$ with the sign change occurring at $I \approx 2 \cdot 10^{-1}$ kg m$^{-2}$ (Fig. 1a). The shape of the net $C(I)$ is a result of the cancellation of the positive longwave (LW) and negative shortwave (SW) contributions. Such a cancellation was already found in early RCE simulations[31] and was recently explained in more detail based on GSRM simulations[10]: With increasing $I$, the opacity of high clouds for LW radiation increases faster than their albedo, giving rise to the positive net $C(I)$, which switches to negative as the albedo keeps increasing with $I$ while the opacity for LW radiation saturates. The surprising increase of the SW $C(I)$ beyond $I > 7$ kg m$^{-2}$ does not result from the high-cloud albedo, but from the diurnal cycle of convection. Such deep convective clouds predominantly occur in

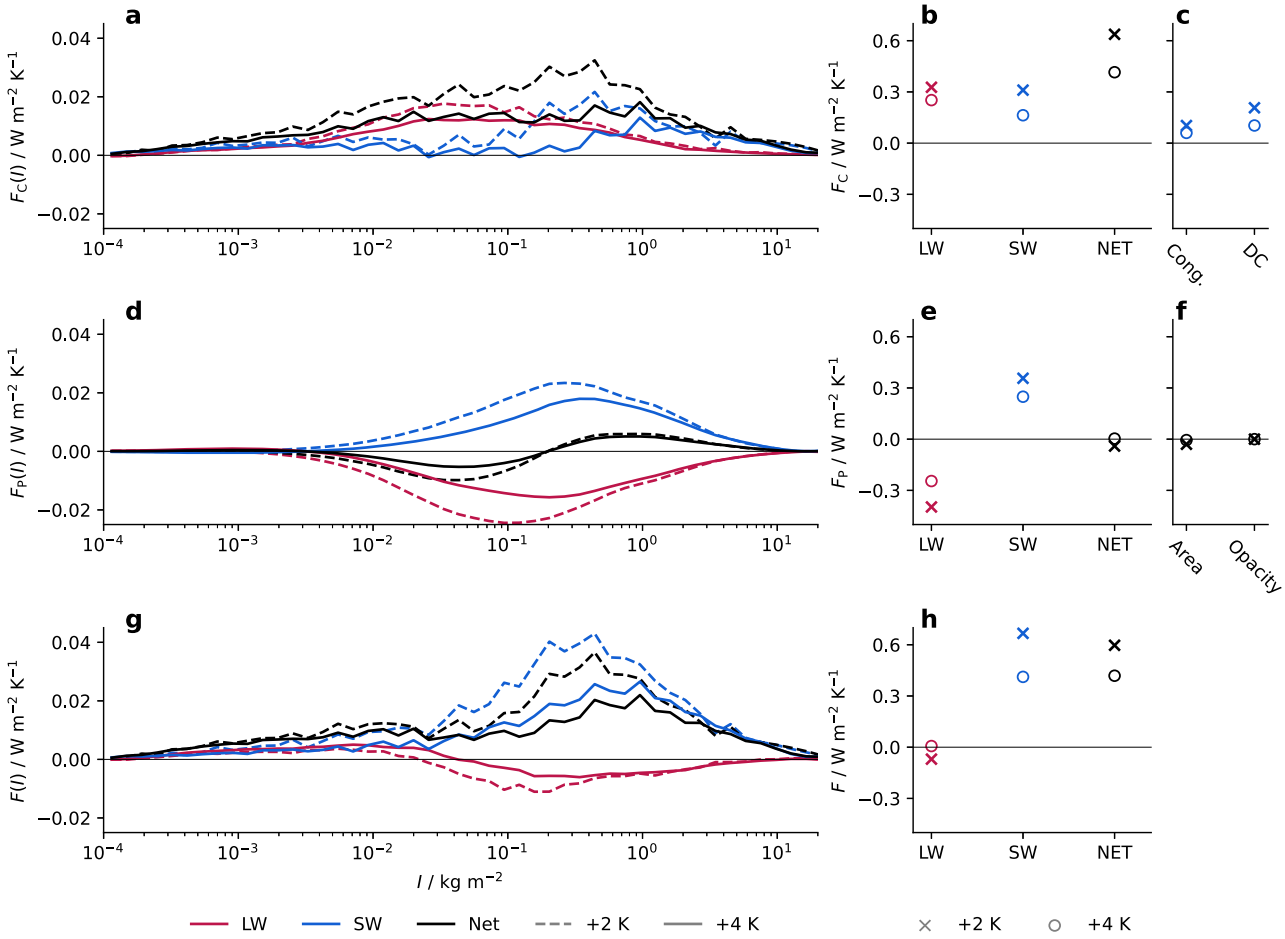



**Fig. 2 | The high-cloud feedback. a** Feedback from changes in the high-cloud radiative effect ($F_C$) as a function of ice water path ($I$) and **b** its sum. **c** The SW $F_C$ partitioned into the feedback from changes in the amount of congestus clouds and changes in the diurnal cycle (DC) of deep convective clouds. **d** Feedback from changes in ice water path frequency ($F_P$) as a function of $I$, **e** its sum and **f** the net $F_P$ partitioned into the feedback from changes in high-cloud area and opacity. **g** Total high-cloud feedback ($F$) as a function of $I$ and **h** its sum. All feedback values are tropical means.

the early morning, which decreases their SW $C(I)$ since the incoming SW radiation is less than for thinner clouds, which occur closer to noon (Fig. S1).

As expected[32,33], the total high-cloud radiative effect ($\overline{C}$) is near-neutral. We calculate $\overline{C}$ as

$$\overline{C} = \sum_I C(I) \cdot P(I). \tag{1}$$

For the control simulation, we get $\overline{C} = 3.7\ \mathrm{W\,m^{-2}}$, which is slightly more positive than earlier estimates[15,34], due to realistic treatment of overlapping low clouds[10] (see 'Methods'). The unrealistically low amount of deep convective clouds in ICON is another cause for a more positive $\overline{C}$. Nevertheless, the magnitude of $\overline{C}$ is still much lower than most $C(I)$, confirming the near-neutrality of $\overline{C}$ from a cancellation of cooling and warming high clouds.

### Positive high-cloud feedback

One advantage of our $I$-framework is that we can analyse whether the feedback is due to changes in $C(I)$ or $P(I)$. The total tropical high-cloud feedback ($F$) is calculated as the change in $\overline{C}$ per unit warming:

$$F = \frac{\Delta\overline{C}}{\Delta T_s} \approx \sum_I \underbrace{P(I)\frac{\Delta C(I)}{\Delta T_s}}_{F_C(I)} + \sum_I \underbrace{\frac{\Delta P(I)}{\Delta T_s} C(I)}_{F_P(I)}, \tag{2}$$

with $T_s$ being the mean surface temperature, and $\Delta$ the difference with respect to the control simulation (see 'Methods'). This linearised chain rule separates the feedback contributions from changes in $P(I)$ ($F_P$) and changes in $C(I)$ ($F_C$).

Our framework differs from other studies that use radiative kernels to isolate cloud feedbacks[16,35]. Using changes in $C$ per unit warming as a measure of cloud feedbacks has been shown to underestimate their magnitude relative to the true cloud feedback, defined as the radiative change caused by cloud properties in isolation[36]. The reason behind this is that changes in $C$ include clear sky effects such as the change in water vapour. However, this does not impact our conclusions, since the magnitude of our feedback values is generally higher than previous estimates, and this discrepancy is explained by the high-cloud response to surface warming (sections 'Fixed high-cloud temperatures' and 'Intensification of the diurnal cycle of deep convection').

The LW $C(I)$ becomes more positive and the SW $C(I)$ becomes less negative with surface warming (Fig. 1c, d), producing positive feedbacks of similar magnitude (Fig. 2a, b). While the LW $\Delta C(I)$ is positive at all $I$, the SW $\Delta C(I)$ is significantly larger than 0 primarily at $I > 1\ \mathrm{kg\,m^{-2}}$, where it reaches about five times the magnitude of its LW counterpart. That the LW and SW contributions to $F_C$ are still of similar magnitude is a result of high values of the SW $\Delta C(I)$ occurring only at less frequent high $I$, whereas the LW $\Delta C(I)$ is also significantly positive at more frequent low $I$. We find that the LW $\Delta C(I)$ results from high-cloud temperatures remaining approximately fixed with surface warming (section 'Fixed high-cloud temperatures'). The SW $\Delta C(I)$ results from a decrease of congestus clouds with surface warming at $I \leq 10^{-1}\ \mathrm{kg\,m^{-2}}$ (Fig. S2) and from changes in the diurnal cycle of deep convective clouds

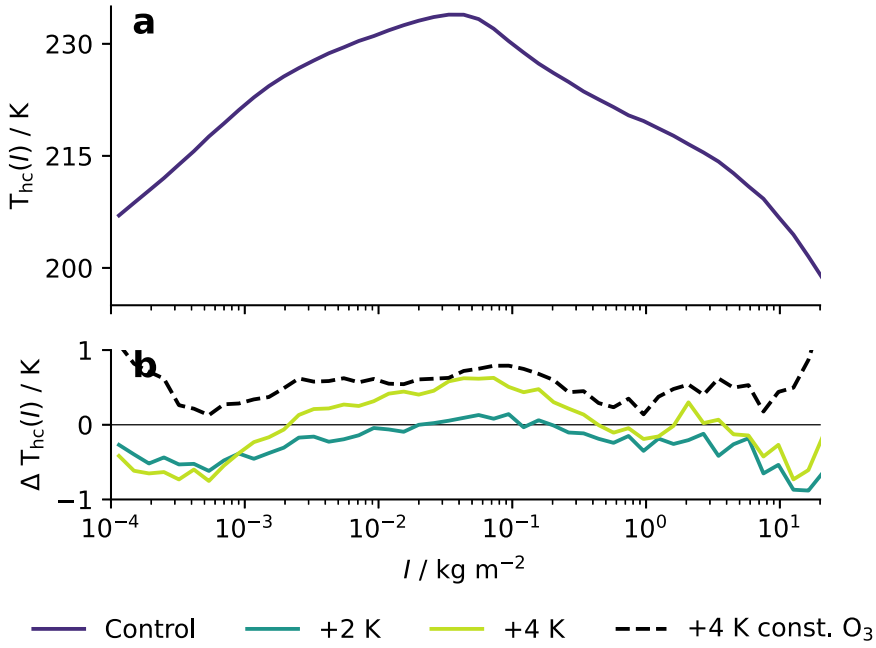



**Fig. 3 | High-cloud temperatures and their change in response to surface warming. a** High-cloud temperature ($T_{hc}$) as a function of ice water path ($I$) and **b** change in high-cloud temperature with respect to the control simulation ($\Delta T_{hc}$).

at $I > 10^{-1}$ kg m$^{-2}$ (section 'Intensification of the diurnal cycle of deep convection').

We partition the SW $F_C$ into contributions from the congestus feedback and the diurnal cycle feedback by summing up $F_C(I)$ over the respective $I$ ranges. This reveals that the diurnal cycle feedback is more than twice as strong as the congestus feedback (Fig. 2c). The positive congestus feedback arises from high clouds in a warmer world being less likely to contain high amounts of liquid condensate at $I \le 10^{-1}$ kg m$^{-2}$, which decreases their average albedo. This feedback is a result of our method for defining high clouds, which includes liquid condensate as part of the high cloud if frozen and liquid condensate sufficiently overlaps (see 'Methods'). If liquid clouds are ignored, the congestus feedback vanishes (Fig. S3). Therefore, we regard the congestus feedback as an artefact of our method for defining high clouds and focus on the diurnal cycle feedback in the following (section 'Intensification of the diurnal cycle of deep convection').

The frequency of high clouds changes with surface warming (Fig. 1e), but the resulting $F_P$ is near-neutral (Fig. 2c, d). The reason for the near-neutral feedback is that the reduction of cooling clouds is cancelled by the reduction of warming clouds, while the increase of the lowest $I$ is not radiatively relevant. Possible explanations for the change in high-cloud frequency are changes in atmospheric stability or cloud radiative heating (section 'Stability iris and radiative heating').

For comparison with previous literature[2,15–17], we partition the net $F_P$ into the more commonly discussed area and the opacity feedbacks[11]. The area feedback is calculated as the overall change in high-cloud fraction times $\overline{C}$. Since $\overline{C}$ is near-neutral, large changes in high-cloud fraction would be required to produce a significant area feedback[15]. However, the overall change in high-cloud fraction remains below 1% K$^{-1}$ for both warming simulations; hence, the area feedback is near zero. The opacity feedback arises since the change in high-cloud fraction is non-uniform across $I$, i.e. it describes the feedback from a shift in the balance between cooling and warming high clouds. The opacity feedback is near neutral for the same reason as the net $F_P$: the reduction of cooling clouds is cancelled by the reduction of warming clouds. Changes in the microphysics of high clouds in response to surface warming can add to the opacity feedback if they affect the opacity of high clouds. This is not the case in our simulations (Fig. S4).

The total tropical high-cloud feedback we derive is positive with 0.60 W m$^{-2}$ K$^{-1}$ (+2 K) and 0.42 W m$^{-2}$ K$^{-1}$ (+4 K). This is a result of both LW $C(I)$ and SW $C(I)$ becoming more positive with surface warming. Within the next sections, we explain and discuss the different feedback components.

## Fixed high-cloud temperatures

The positive LW $F_C$ results from tropical high-cloud temperatures ($T_{hc}$) remaining approximately fixed despite surface warming. The binned $T_{hc}(I)$ reveals that deep convective clouds ($I > 1$ kg m$^{-2}$) are coldest, anvils (1 kg m$^{-2} \ge I > 10^{-2}$ kg m$^{-2}$) are about 30 K warmer and thin cirrus ($I \le 10^{-2}$ kg m$^{-2}$) are almost as cold as the deep convective clouds (Fig. 3a). This shape of $T_{hc}(I)$ remains remarkably fixed despite surface warming. The change in $T_{hc}(I)$ with respect to the control simulation is below 1 K for all $I$ (Fig 3b). The change of the average $T_{hc}(I)$ weighted with $P(I)$ per degree of surface warming is −0.17 K K$^{-1}$ (+2 K) and −0.06 K K$^{-1}$ (+4 K).

Our finding of approximately fixed high-cloud temperatures agrees well with the fixed anvil temperature (FAT) theory[12], but disagrees with most GCMs, which predict high clouds to warm at about 0.33 K K$^{-1}$ as surface temperatures increase, which gave rise to the proportionately higher anvil temperature (PHAT) theory[13,14]. Within those GCM simulations, ozone is usually prescribed to remain constant on pressure levels despite surface warming[37,38]. It has been argued that such treatment of ozone might cause an unrealistic warming of tropical high clouds[39]. We test this hypothesis with an additional +4 K warming simulation for which we prescribe the ozone profile from the control simulation to remain constant on pressure levels (see 'Methods'). We find that in this case, high-cloud temperatures do indeed slightly increase with surface warming at 0.09 K K$^{-1}$ (Fig. 3). If ozone is prescribed, the ozone profile cannot rise to higher altitudes together with the temperature profile as the surface warms, resulting in higher ozone concentrations in the upper troposphere and tropopause region and hence higher temperatures (Fig. S5). This finding emphasises the importance of interactive ozone schemes and casts doubt on the PHAT theory. However, prescribed ozone only explains about half of the difference between the high-cloud temperature change in GCMs and our simulations. The remaining discrepancy might be explained by differences in the method used to diagnose $T_{hc}$ or by fundamental differences between GCMs and GSRMs.

Our estimates of the LW $F_C$ of 0.33 W m$^{-2}$ K$^{-1}$ (+2 K) and 0.25 W m$^{-2}$ K$^{-1}$ (+4 K) lie at the upper bound of previous estimates of the high-cloud altitude feedback. The global mean feedback value from the WCRP assessment can be directly compared to our tropical mean values, since GCMs suggest that the high-cloud altitude feedback is of similar

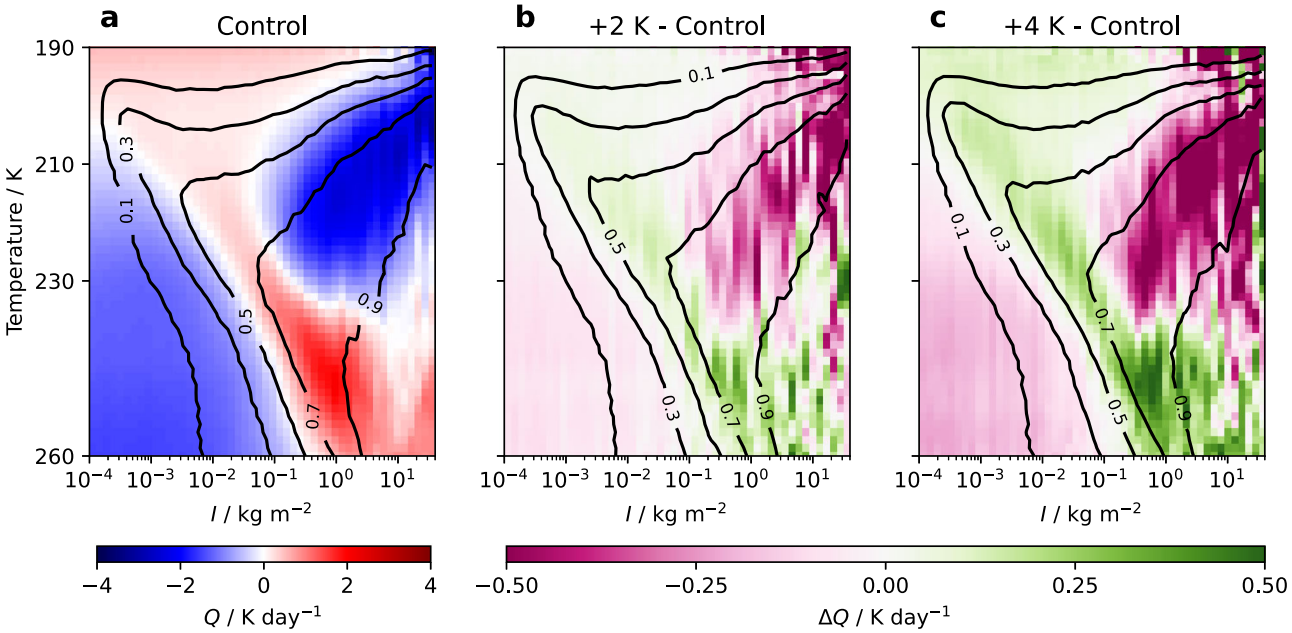



**Fig. 4 | Radiative heating and its change in response to surface warming. a** Radiative heating rate ($Q$) binned by temperature and ice water path ($I$) for the control run, **b**, **c** change in radiative heating rate ($\Delta Q$) with respect to the control simulation. The contour lines depict cloud fraction.

magnitude in the tropics and the rest of the world[2,14]. The WCRP feedback estimate of 0.2 ± 0.1 W m$^{-2}$ K$^{-1}$ is based on their ensemble of GCM simulations, but they also derive a feedback estimate of 0.35 ± 0.2 W m$^{-2}$ K$^{-1}$ from an observational study[40]. Our results are closer to that observational estimate than to the one from GCMs. This is a consequence of fixed high-cloud temperatures in our simulations, rather than the slight warming simulated by most GCMs, which may be due to unrealistic ozone treatment.

### Stability iris and radiative heating

While we do find the expected[41–43] decrease of anvil clouds (1 kg m$^{-2}$ ≥ $I$ > $10^{-2}$ kg m$^{-2}$) in response to surface warming, the feedback resulting from changes in high-cloud frequency is near-neutral. The area feedback is near-neutral, since the total area change and the mean high-cloud radiative effect are small, which agrees with observational estimates[15–17], but contradicts the negative WCRP feedback estimate. The opacity feedback, not discussed by the WCRP, is also near-neutral in our simulations, since clouds with negative and positive $C(I)$ reduce equally in frequency (Fig. 2c).

Doubts about a negative feedback from a reduction of anvil clouds are supported by recent cloud-resolving RCE simulations, which also yield a near-neutral area feedback, but a positive opacity feedback of 0.07 W m$^{-2}$ K$^{-1}$[11]. The shape of $\Delta P(I)$ from the RCE simulations resembles our result, but the decrease in frequency mostly affects thicker clouds with a negative $C(I)$ in the RCE simulations, which explains their positive opacity feedback. In contrast, the response of thin clouds with a positive $C(I)$ to surface warming varies substantially across models in the RCE ensemble. The decrease of such thin clouds in response to surface warming that we find in our simulations may therefore be model-specific, rather than a robust discrepancy to the RCE results.

Judging from the shape of $\Delta P(I)$ (Fig. 1e), there seem to be two counteracting mechanisms at work in our simulations that drive the change of high-cloud frequency in response to surface warming: one that increases thin cirrus and one that decreases anvil clouds.

The stability iris[41–44] is a mechanism associated with a reduction of anvil clouds in response to warming. The physical thinking behind the stability iris is that the horizontal divergence detraining anvil clouds from deep convection is constrained by radiatively driven convergence in clear-sky regions via mass balance. As atmospheric stability increases, clear-sky convergence and hence anvil clouds are expected to decrease. We find that a stability iris exists in our simulations as clear-sky convergence decreases with surface warming at 0.006 day$^{-1}$ K$^{-1}$ (Fig. S6). However, this decrease is smaller than the 0.013 day$^{-1}$ K$^{-1}$ found in cloud-resolving RCE simulations[42] or the 0.016 day$^{-1}$ K$^{-1}$ from GCM RCE simulations[41]. A possible reason for this disagreement is that we are using all-sky radiative fluxes in cloud-free regions to calculate radiative subsidence (see 'Methods'), while the above-mentioned studies use clear-sky radiative fluxes over the entire domain, which we did not save.

We hypothesise that an increase in radiative heating in cirrus clouds (Fig. 4) might prolong cirrus lifetimes, which would explain their increased frequency at higher surface temperatures. Our simulations confirm basic physical considerations[45] that the magnitude of radiative heating in clouds increases with surface warming (Fig. 4). As the surface warms, clouds rise isothermally to lower pressure and hence lower density, which increases the magnitude of heating rates (Fig. S7). Cirrus lifetimes are prolonged by radiative heating that causes the cloud to rise and hence keeps it in a supersaturated environment[46]. As radiative heating in cirrus clouds increases with surface warming, cirrus are lifted to colder temperatures (Fig. 3b), which should increase their lifetime.

### Intensification of the diurnal cycle of deep convection

A major advancement of GSRMs is that they can simulate a realistic diurnal cycle of deep convection, something GCMs struggle with[7,47]. We use the Chalmers Cloud Ice Climatology (CCIC)[48,49] to compare the diurnal cycle of deep convection from our aquaplanet simulations to the diurnal cycle over oceans. We define deep convective clouds as grid cells with $I$ > 1 kg m$^{-2}$, in agreement with earlier studies[50]. The aquaplanet simulations reproduce the two peaks of deep convective clouds, but the early morning peak is more pronounced than the afternoon peak compared to CCIC (Fig. 5). The afternoon peak is assumed to be intensified by diurnal SST variations[51,52], which would explain why it is less pronounced in our aquaplanet simulations with fixed SST.

We find that the positive SW $F_C$ at $I$ > 0.1 kg m$^{-2}$ is due to a more pronounced diurnal cycle of deep convection. Deep convection during daytime reduces in response to surface warming, and so do the clouds produced by deep convection. This is most pronounced for deep convective clouds (Fig. 5), but also affects thick anvil clouds with 0.1 kg m$^{-2}$ < $I$ < 1 kg m$^{-2}$ (Fig. S1). This means that the overall decrease of clouds produced by

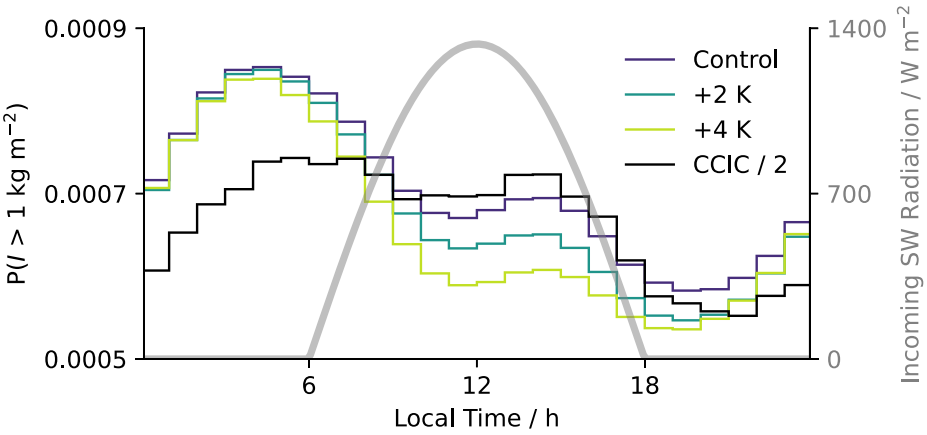



**Fig. 5 | Diurnal cycle of deep convective clouds.** Frequency of occurrence ($P$) of deep convective clouds with ice water path ($I$) higher than 1 kg m$^{-2}$ for every hour and incoming SW radiation. Values of CCIC are divided by two to facilitate the comparison of the diurnal cycle of deep convection, since ICON has approximately half as many deep convective clouds as CCIC.

deep convection (Fig. 1e) mostly happens during the day. As clouds produced by deep convection become less frequent during the day, they receive less solar radiation and hence reflect less, which explains their weaker SW $C(I)$.

The feedback associated with changes in the diurnal cycle of tropical deep convection has received limited attention, even though our results suggest that it substantially contributes to the positive tropical high-cloud feedback. The SW $F_C$ resulting from changes in the diurnal cycle of deep convection is 0.2 W m$^{-2}$ K$^{-1}$ (+2 K) and 0.1 W m$^{-2}$ K$^{-1}$ (+4 K). Further studies are necessary to test whether the diurnal cycle feedback also exists over land. If it holds only over tropical oceans, which our simulations are representative of, the feedback must be scaled by the ocean fraction in the tropics (0.74), which yields 0.15 W m$^{-2}$ K$^{-1}$ (+2 K) and 0.074 W m$^{-2}$ K$^{-1}$ (+4 K) for the tropical feedback. The non-linearity of the diurnal cycle feedback is caused by thick anvils with 0.1 kg m$^{-2}$ < $I$ < 1 kg m$^{-2}$ (Fig. 2a). Those clouds reduce substantially during the day in the +2 K simulation, while their response is more muted in +4 K simulation (Fig. S1).

Our analysis suggests that the amplification of the diurnal cycle of deep convection results from intensified radiative heating in clouds in response to surface warming. Radiative heating has been shown to drive the diurnal cycle of deep convection over the ocean[53–55]. The peak of deep convection in the early morning hours is caused by LW cooling of high clouds communicated to the surroundings via gravity waves, which leads to a destabilisation of the atmosphere, favouring deep convection. During the day, SW heating in high clouds stabilises the atmosphere and leads to a suppression of deep convection. With radiative heating being a key driver of the diurnal cycle of deep convection, it seems reasonable to assume that the intensified radiative heating (Fig. 4) causes the intensified diurnal cycle of deep convection.

It remains an open question how the presence of land might influence changes in the diurnal cycle of deep convection. Convection over land may respond differently to surface warming, since its diurnal cycle is strongly controlled by SW surface heating[56]. In addition, land-sea contrasts that drive local circulations may further modulate changes in the diurnal cycle of deep convection. Nevertheless, the increasing magnitude of radiative heating is independent of the surface type[45], suggesting that the mechanism outlined above may be universal.

The robustness of changes in the diurnal cycle of deep convection in response to surface warming to differences in the remaining parameterisations in GSRMs should be tested. Tropical high clouds are known to be sensitive to the parameterisations of cloud microphysics[57,58] and turbulence[59]. Therefore, the amplification of the diurnal cycle of deep convection in response to surface warming that we find may depend on those parameterisations. Since our explanation for changes in the diurnal cycle of deep convection does not involve rotation or global scales, conceptually simple and computationally cheap RCE simulations might be sufficient to test this.

## Discussion

Resolving the spectrum of high clouds, ranging from thin cirrus to thick deep convective clouds, allows us to reassess the tropical high-cloud feedback. Our GSRM simulations reveal that the tropical high-cloud feedback consists of three parts, ranging from previously known to newly identified: A positive longwave feedback from fixed high-cloud temperatures, a near-neutral feedback from changes in high-cloud frequency, and a positive shortwave feedback from an intensified diurnal cycle of deep convection.

That high-cloud temperatures remain fixed despite surface warming agrees with theory[12], but disagrees with most GCMs, which predict a slight warming of high clouds[13,14]. Therefore, the resulting feedback is more positive in our simulations than in GCMs. We find that this discrepancy is partly due to the unrealistic treatment of ozone within GCMs.

The anticipated reduction of tropical high clouds with surface warming, thought to be driven by an increase in atmospheric stability[41], affects thin (warming) and thick (cooling) clouds equally in our simulation. Therefore, we find the feedback from changes in high-cloud frequency to be near neutral, rather than negative, as suggested by the WCRP assessment. Such doubts about the WCRP estimate are supported by recent RCE simulations[11] and observational estimates[15–17].

The feedback from changes in the diurnal cycle of clouds has received limited attention, but our results suggest that it can be substantial. As the surface warms, thick and reflective clouds produced by deep convection occur less frequently during the day and more frequently during the night, and hence reflect less sunlight. We hypothesise that this change in the diurnal cycle of deep convection is driven by the increase of radiative heating in clouds with surface warming, consistent with the strong coupling between radiative heating in clouds and deep convection[53]. The broad agreement between the diurnal cycle of deep convection from our aquaplanet simulations and the observed diurnal cycle over oceans lends credibility to the plausibility of such a feedback. Nevertheless, targeted modelling studies are required to investigate the mechanism causing a reduction of daytime deep convection, and observational analyses will be essential to assess whether this feedback operates in the real climate system.

Overall, our results suggest that a positive tropical high-cloud feedback seems more plausible than the near-neutral feedback suggested by the WCRP assessment, which implies a higher climate sensitivity.

## Methods

### Aquaplanet simulations

We use version 2024.10 of ICON, which is open source and available from GitLab. We use a vertical grid with 90 levels, which are increasingly fine-spaced towards the surface. The SST is prescribed to follow the zonally symmetric Qobs distribution[24], with maximum temperatures at the equator and minimum temperatures at the poles.

For the control simulation, we run 6 months of spin-up, which is sufficient for the model to reach a stationary state (not shown). To save

computing time, we initialise the spin-up simulations of the +2 K, the +4 K and the +4 K with constant ozone simulations from the control spin-up. This allows us to shorten their spin-up simulations to 3 months.

We use 3 months of simulation of the control, the +2 K, the +4 K runs for our analysis. This is sufficiently long to reach a statistically stable state for $\Delta P(I)$, which we found to be the most fragile quantity in our analysis (Fig. S8). We only use 1 month of simulation for the +4 K run with constant ozone. Changes in high cloud temperature are more robust, and hence 1 month is sufficient to reach a statistically stable state.

All the data that we use is instantaneous. Full 3D atmospheric profiles are saved at 0 UTC every day, and 2D variables are saved hourly. Saving 3D profiles once a day is sufficient since the aquaplanet is uniform along latitudes.

### Handling big data

To reduce the amount of data required for our analysis, we draw random samples from the model output. We randomly sample $10^7$ atmospheric profiles from within the tropics (20°S to 20°N) for every simulation, which proves sufficient to capture the statistics of the data (not shown). Those samples are used for calculating $C$ and $T_{\mathrm{hc}}$, which require 3D profiles. For the analysis of the stability iris and the heating rates, we interpolate a subsample of $10^6$ 3D profiles on temperature levels.

For the histograms within our analysis (Fig. 1b, e and Fig. 5), we use the entire 2D data to achieve maximum accuracy.

### High-cloud radiative effect

For the calculation of $C$, we define high clouds as any cloud that contains frozen condensate. We consider liquid condensate to be part of the high cloud if frozen and liquid condensate sufficiently overlap within the column[10,60]. This avoids artificial separation of liquid and frozen clouds, which is most obvious for deep convection, where liquid and frozen condensate are always part of the same cloud and cannot exist without the other phase.

We calculate three radiative fluxes: The all-sky flux ($F_{\mathrm{allsky}}$), which includes all condensate, the wet-sky flux ($F_{\mathrm{wetsky}}$), which only sees liquid condensate and the clear-sky flux ($F_{\mathrm{clearsky}}$), which does not see any condensate.

We calculate $C$ as the difference in the net radiative flux with and without the high cloud at the top of the atmosphere :

$$C = F_{\mathrm{allsky}} - F_{\mathrm{nohcld}}, \tag{3}$$

where the flux without the high cloud ($F_{\mathrm{nohcld}}$) either includes liquid condensate or not, depending on whether the liquid phase is part of the high cloud:

$$F_{\mathrm{nohcld}} = \begin{cases} F_{clearsky}, & \text{if } c = 1, \\ F_{wetsky}, & \text{if } c = 0. \end{cases} \tag{4}$$

Here, $c$ represents the connectedness of the liquid and frozen cloud condensate within the column, with a value of 1 indicating that the two are connected and 0 otherwise.

We determine whether liquid condensate ($q_{\mathrm{l}}$) and frozen condensate ($q_{\mathrm{f}}$) are connected, based on the gap between their respective maxima. To this end, we calculate the height ($z$) of the maximum frozen and liquid condensate for every column:

$$z_{\mathrm{l}} = z|_{\max(q_{\mathrm{l}})}, \tag{5}$$

$$z_{\mathrm{f}} = z|_{\max(q_{\mathrm{f}})}. \tag{6}$$

If we can find a grid cell between $z_{\mathrm{f}}$ and $z_{\mathrm{l}}$ where both liquid and frozen condensate are less than 5% times a tuning factor of their maximum, we consider both phases to be unconnected:

$$c = \begin{cases} 0, & \exists\, z \in [z_{\mathrm{l}}, z_{\mathrm{f}}] : (q_{\mathrm{l}} < 0.05 \cdot \left(\frac{z_{\mathrm{k}}}{z_{\mathrm{m}}}\right)^7 \cdot \max(q_{\mathrm{l}})) \wedge (q_{\mathrm{f}} < 0.05 \cdot \left(\frac{z_{\mathrm{k}}}{z_{\mathrm{m}}}\right)^7 \cdot \max(q_{\mathrm{f}})), \\ 1, & \text{Else}, \end{cases} \tag{7}$$

where $z_{\mathrm{k}}$ is the average difference between $z_{\mathrm{l}}$ and $z_{\mathrm{f}}$ of the respective simulation and $z_{\mathrm{m}}$ is the average of $z_{\mathrm{k}}$ over all three simulations. The SW $F_{\mathrm{C}}$ is the only feedback component that is sensitive to the threshold chosen to decide whether frozen and liquid clouds are connected (Fig. S9). Since the sign of the SW $F_{\mathrm{C}}$ is robust, this does not affect our conclusions.

The tuning factor $\left(\frac{z_{\mathrm{k}}}{z_{\mathrm{m}}}\right)^7$ is necessary because clouds extend further up with warming. This means there will be a higher chance of finding a grid box with less than the fraction of condensate required for $c = 1$, which increases the fraction of unconnected liquid clouds with warming (Fig. S10). More liquid cloud below the high clouds would decrease the SW $C(I)$ and hence create a SW feedback[10]. We consider such a feedback to be artificial, since the mean liquid cloud fraction does not increase with warming (Fig. S10). To avoid such an artificial feedback, we keep the liquid cloud fraction constant at each $I$ by using the tuning factor.

Introducing the $F_{\mathrm{wetsky}}$ as an additional diagnostic variable in ICON is necessary to properly distinguish high, frozen clouds from low, liquid clouds. This mainly becomes important for anvil and cirrus clouds, which are independent of the lower liquid clouds. If $F_{\mathrm{wetsky}}$ is not available, an alternative approach can be to disregarding gridcells with overlapping high and low clouds for low $I$[11]. However, this leads to an underestimation of $C(I)$ for those clouds[10].

The $I$ frequency distribution $P(I)$ used to calculate the total high-cloud radiative effect $\overline{C}$ (Eq. (1)) should be interpreted as the $I$-resolved high-cloud fraction. That means $\overline{C}$ is the average high-cloud radiative effect across the tropics, including areas without high clouds.

### Feedback partitioning

The complete equation for the partitioning of the total high-cloud feedback, $F$, also includes a non-linear term:

$$F = \frac{\Delta \overline{C}}{\Delta T_{\mathrm{s}}} = \sum_I \underbrace{\frac{\Delta P(I)}{\Delta T_{\mathrm{s}}} C(I)}_{F_{\mathrm{P}}(I)} + \sum_I \underbrace{P(I) \frac{\Delta C(I)}{\Delta T_{\mathrm{s}}}}_{F_{\mathrm{C}}(I)} + \sum_I \underbrace{\frac{\Delta P(I)}{\Delta T_{\mathrm{s}}} \frac{\Delta C(I)}{\Delta T_{\mathrm{s}}}}_{\text{non-linear}}. \tag{8}$$

We neglect this non-linear term, since it is one order of magnitude smaller than both linear terms. Both $C(I)$ and $P(I)$ are taken from the control simulation.

### High-cloud temperature

We calculate $T_{\mathrm{hc}}$ as

$$T_{\mathrm{hc}} = \min(T|_{\max q_{\mathrm{i}}}, T_{\mathrm{b}}), \tag{9}$$

with $T|_{\max q_{\mathrm{i}}}$ being the temperature at maximum cloud ice ($q_{\mathrm{i}}$) concentration, and $T_{\mathrm{b}}$ being brightness temperature. This formulation of $T_{\mathrm{hc}}$ has the advantage that it captures thin high-clouds which are semi-transparent to LW radiation and can hence be applied to clouds with any $I$[10].

### Stability iris analysis

The physical thinking behind the stability iris is that the horizontal divergence ($\nabla_{\mathrm{h}} \mathbf{v}_{\mathrm{cld}}$), which detrains anvil clouds from deep convection, is constrained by horizontal convergence in clear-sky regions ($-\nabla_{\mathrm{h}} \mathbf{v}_{\mathrm{clear}}$) via mass balance[41]. This convergence is a result of the clear-sky subsidence profile ($\omega_{\mathrm{clear}}$), which balances the radiative cooling ($Q$):

$$\nabla_{\mathrm{h}} \mathbf{v}_{\mathrm{cld}} = -\nabla_{\mathrm{h}} \mathbf{v}_{\mathrm{clear}} = \frac{\partial \omega_{\mathrm{clear}}}{\partial_z} \approx -\frac{\partial}{\partial_z} \frac{Q}{S}, \tag{10}$$

where $S$ is static stability and $z$ is height. We neglect latent heating in line with earlier studies[41,44].

We calculate $Q$ as:

$$Q = \frac{1}{\rho c_p}\frac{dF}{dz}, \tag{11}$$

where $\rho$ is air density, $c_p$ specific heat capacity of air and $F$ the radiative flux.

The static stability ($S$) is calculated as the difference between the dry lapse rate and the lapse rate:

$$S = \Gamma_d - \Gamma = \frac{g}{c_p} - \frac{dT}{dz}, \tag{12}$$

where $g$ is the gravitational constant.

Most previous studies analysing the stability iris use 3D clear-sky radiative fluxes[41,42], whereas we only store 3D all-sky radiative fluxes due to disk storage constraints. Therefore, we define clear-sky profiles as profiles with $I < 10^{-2}\,\mathrm{kg\,m^{-2}}$, where $C(I)$ becomes sufficiently small (Fig. 1a). Our key findings do not rely on this threshold.

From the mean clear-sky profiles of $Q$ and $S$, we calculate $\omega_{clear}$:

$$\omega_{clear} = -\frac{Q}{S}. \tag{13}$$

The clear-sky convergence is then calculated as the vertical derivative of $\omega$ (Eq. (10)). To disregard the noise in the clear-sky convergence profile, we use a third-order Savitzky-Golay filter to smooth $\omega$ before calculating the derivative.

## Data availability

The DARDAR data is available from https://www.icare.univ-lille.fr/dardar/399data-access/data-access/ and 2C-ICE data from https://cloudsat.cira.colostate.edu/data-products/2c-ice. The data to reproduce the figures and numbers from this paper is available from https://doi.org/10.5281/zenodo.17472593[61].

## Code availability

The code to reproduce the figures and numbers from this paper is available from https://doi.org/10.5281/zenodo.17472875[62].

Received: 16 March 2026; Accepted: 7 June 2026;
Published online: 20 June 2026

## References

1. Gasparini, B., Sullivan, S. C., Sokol, A. B., Kärcher, B., Jensen, E. & Hartmann, D. L. Opinion: Tropical cirrus –from micro-scale processes to climate-scale impacts. *Atmos. Chem. Phys* **23**, 15413–15444 (2023).
2. Sherwood, S. C. et al. An assessment of Earth's climate sensitivity using multiple lines of evidence. *Rev. Geophys.* **58**, e2019RG000678 (2020).
3. Stevens, B. & Bony, S. What are climate models missing? *Science* **340**, 1053–1054 (2013).
4. Sanderson, B. M., Piani, C., Ingram, W. J., Stone, D. A. & Allen, M. R. Towards constraining climate sensitivity by linear analysis of feedback patterns in thousands of perturbed-physics GCM simulations. *Clim. Dyn.* **30**, 175–190 (2008).
5. Schär, C. et al. Kilometer-scale climate models: prospects and challenges. *Bull. Am. Meteorol. Soc*. https://journals.ametsoc.org/view/journals/bams/101/5/bams-d-18-0167.1.xml (2020).
6. Satoh, M. et al. Global cloud-resolving models. *Curr. Clim. Change Rep.* **5**, 172–184 (2019).
7. Stevens, B. et al. The added value of large-eddy and storm-resolving models for simulating clouds and precipitation. *J. Meteorol. Soc. Jpn. Ser. II* **98**, 395–435 (2020).
8. Lang, T., Naumann, A. K., Stevens, B. & Buehler, S. A. Tropical free-tropospheric humidity differences and their effect on the clear-sky radiation budget in global storm-resolving models. *J. Adv. Model. Earth Syst.* **13**, e2021MS002514 (2021).
9. Turbeville, S. M., Nugent, J. M., Ackerman, T. P., Bretherton, C. S. & Blossey, P. N. Tropical cirrus in global storm-resolving models: 2. Cirrus life cycle and top-of-atmosphere radiative fluxes. *Earth Space Sci.* **9**, e2021EA001978 (2022).
10. Deutloff, J., Buehler, S. A., Brath, M. & Naumann, A. K. Insights on tropical high-cloud radiative effect from a new conceptual model. *J. Adv. Model. Earth Syst.* **17**, e2024MS004615 (2025).
11. Sokol, A. B., Wall, C. J. & Hartmann, D. L. Greater climate sensitivity implied by anvil cloud thinning. *Nat. Geosci*. 1–6. https://www.nature.com/articles/s41561-024-01420-6 (2024).
12. Hartmann, D. L. & Larson, K. An important constraint on tropical cloud—climate feedback. *Geophys. Res. Lett.* **29**, 12–1–12–4 (2002).
13. Zelinka, M. D. & Hartmann, D. L. Why is longwave cloud feedback positive? *J. Geophys. Res. Atmos.* **115**, https://doi.org/10.1029/2010JD013817 (2010).
14. Ceppi, P., Brient, F., Zelinka, M. D. & Hartmann, D. L. Cloud feedback mechanisms and their representation in global climate models. *WIREs Clim. Change* **8**, e465 (2017).
15. McKim, B., Bony, S. & Dufresne, J.-L. Weak anvil cloud area feedback suggested by physical and observational constraints. *Nat. Geosci.* 1–6. https://www.nature.com/articles/s41561-024-01414-4 (2024).
16. Raghuraman, S. P., Medeiros, B. & Gettelman, A. Observational quantification of tropical high cloud changes and feedbacks. *J. Geophys. Res. Atmos.* **129**, e2023JD039364 (2024).
17. Wilson Kemsley, S., Nowack, P. & Ceppi, P. Climate models underestimate global decreases in high-cloud amount with warming. *Geophys. Res. Lett.* **52**, e2024GL113316 (2025).
18. Hohenegger, C. et al. ICON-Sapphire: simulating the components of the Earth system and their interactions at kilometer and subkilometer scales. *Geosci. Model Dev.* **16**, 779–811 (2023).
19. Smagorinsky, J. General circulation experiments with the primitive equations. *Mon. Weather Rev*. https://journals.ametsoc.org/view/journals/mwre/91/3/1520-0493_1963_091_0099_gcewtp_2_3_co_2.xml (1963).
20. Baldauf, M. et al. Operational convective-scale numerical weather prediction with the COSMO model: description and sensitivities. *Mon. Weather Rev*. https://journals.ametsoc.org/view/journals/mwre/139/12/mwr-d-10-05013.1.xml (2011).
21. Cariolle, D. & Teyssèdre, H. A revised linear ozone photochemistry parameterization for use in transport and general circulation models: multi-annual simulations. *Atmos. Chem. Phys.* **7**, 2183–2196 (2007).
22. Bravo, A. P., Klocke, D. & Stevens, B. Horizontal grid spacing convergence of aquaplanet experiments. https://www.authorea.com/users/811273/articles/1212740-horizontal-grid-spacing-convergence-of-aquaplanet-experiments?commit=91e2cafa248a22f936c24bcad585c8096ec0fd01 (2024).
23. Blackburn, M. et al. The aqua-planet experiment (APE): CONTROL SST simulation. *J. Meteorol. Soc. Jpn. Ser. II* **91**, 17–56 (2013).
24. Neale, R. B. & Hoskins, B. J. A standard test for AGCMs including their physical parametrizations: I: the proposal. *Atmos. Sci. Lett.* **1**, 101–107 (2000).
25. Stauffer, C. L. & Wing, A. A. Explicitly resolved cloud feedbacks in the radiative-convective equilibrium model intercomparison project. *J. Adv. Model. Earth Syst.* **15**, e2023MS003738 (2023).
26. Medeiros, B., Stevens, B. & Bony, S. Using aquaplanets to understand the robust responses of comprehensive climate models to forcing. *Clim. Dyn.* **44**, 1957–1977 (2015).
27. Deng, M., Mace, G. G., Wang, Z. & Okamoto, H. Tropical Composition, Cloud and Climate Coupling Experiment validation for cirrus cloud profiling retrieval using CloudSat radar and CALIPSO lidar. *J.*

*Geophys. Res. Atmos.* **115**, https://doi.org/10.1029/2009JD013104 (2010).
28. Delanoë, J. & Hogan, R. J. Combined CloudSat-CALIPSO-MODIS retrievals of the properties of ice clouds. *J. Geophys. Res. Atmos.* **115**, https://doi.org/10.1029/2009JD012346 (2010).
29. Gasparini, B., Atlas, R., Voigt, A., Krämer, M. & Blossey, P. N. Tropical cirrus evolution in a kilometer-scale model with improved ice microphysics. *Atmos. Chem. Phys.* **25**, 9957–9979 (2025).
30. Gasparini, B., Sokol, A. B., Wall, C. J., Hartmann, D. L. & Blossey, P. N. Diurnal differences in tropical maritime anvil cloud evolution. *J. Clim.* **35**, 1655–1677 (2022).
31. Manabe, S. & Strickler, R. F. Thermal equilibrium of the atmosphere with a convective adjustment. *J. Atmos. Sci.* **21**, 361–385 (1964).
32. Hartmann, D. L. & Berry, S. E. The balanced radiative effect of tropical anvil clouds. *J. Geophys. Res. Atmos.* **122**, 5003–5020 (2017).
33. Hartmann, D. L., Moy, L. A. & Fu, Q. Tropical convection and the energy balance at the top of the atmosphere. *J. Clim.* **14**, 4495–4511 (2001).
34. L'Ecuyer, T. S., Hang, Y., Matus, A. V. & Wang, Z. Reassessing the effect of cloud type on earth's energy balance in the age of active spaceborne observations. Part I: top of atmosphere and surface. *J. Clim.* **32**, 6197–6217 (2019).
35. Zelinka, M. D., Zhou, C. & Klein, S. A. Insights from a refined decomposition of cloud feedbacks. *Geophys. Res. Lett.* **43**, 9259–9269 (2016).
36. Soden, B. J., Broccoli, A. J. & Hemler, R. S. On the use of cloud forcing to estimate cloud feedback. *J. Clim.* **17**, 3661–3665 (2004).
37. Taylor, K. E., Stouffer, R. J. & Meehl, G. A. An overview of CMIP5 and the experiment design. *Bull. Am. Meteorol. Soc*. https://journals.ametsoc.org/view/journals/bams/93/4/bams-d-11-00094.1.xml (2012).
38. Eyring, V. et al. Overview of the Coupled Model Intercomparison Project Phase 6 (CMIP6) experimental design and organization. *Geosci. Model Dev.* **9**, 1937–1958 (2016).
39. Seidel, S. D. & Yang, D. Temperatures of anvil clouds and radiative tropopause in a wide array of cloud-resolving simulations. *J. Clim*. https://journals.ametsoc.org/view/journals/clim/35/24/JCLI-D-21-0962.1.xml (2022).
40. Vaillant de Guélis, T. et al. Space lidar observations constrain longwave cloud feedback. *Sci. Rep.* **8**, 16570 (2018).
41. Bony, S. et al. Thermodynamic control of anvil cloud amount. *Proc. Natl. Acad. Sci.* **113**, 8927–8932 (2016).
42. Jeevanjee, N. Three rules for the decrease of tropical convection with global warming. *J. Adv. Model. Earth Syst.* **14**, e2022MS003285 (2022).
43. Saint-Lu, M., Bony, S. & Dufresne, J.-L. Observational evidence for a stability iris effect in the tropics. *Geophys. Res. Lett.* **47**, e2020GL089059 (2020).
44. Saint-Lu, M., Bony, S. & Dufresne, J.-L. Clear-sky control of anvils in response to increased CO2 or surface warming or volcanic eruptions. *npj Clim. Atmos. Sci.* **5**, 1–8 (2022).
45. Gasparini, B., Mandorli, G., Stubenrauch, C. & Voigt, A. Basic physics predicts stronger high cloud radiative heating with warming. *Geophys. Res. Lett.* **51**, e2024GL111228 (2024).
46. Hartmann, D. L., Gasparini, B., Berry, S. E. & Blossey, P. N. The life cycle and net radiative effect of tropical anvil clouds. *J. Adv. Model. Earth Syst.* **10**, 3012–3029 (2018).
47. Song, J. et al. Realistic precipitation diurnal cycle in global convection-permitting models by resolving mesoscale convective systems. *Geophys. Res. Lett.* **51**, e2024GL109945 (2024).
48. Amell, A., Pfreundschuh, S. & Eriksson, P. The Chalmers Cloud Ice Climatology: retrieval implementation and validation. *Atmos. Meas. Tech.* **17**, 4337–4368 (2024).
49. Pfreundschuh, S. et al. The Chalmers Cloud Ice Climatology: a novel robust climate record of frozen cloud hydrometeor concentrations. *J. Geophys. Res. Atmos.* **130**, e2024JD042618 (2025).
50. Bolot, M. et al. Kilometer-scale global warming simulations and active sensors reveal changes in tropical deep convection. *npj Clim. Atmos. Sci.* **6**, 1–8 (2023).
51. Ruppert, J. H. & Johnson, R. H. On the cumulus diurnal cycle over the tropical warm pool. *J. Adv. Model. Earth Syst.* **8**, 669–690 (2016).
52. Bellenger, H., Takayabu, Y. N., Ushiyama, T. & Yoneyama, K. Role of diurnal warm layers in the diurnal cycle of convection over the tropical Indian Ocean during MISMO. *Mon. Weather Rev.* **138**, 2426–2433 (2010).
53. Ruppert, J. H. & Hohenegger, C. Diurnal circulation adjustment and organized deep convection. *J. Clim*. https://journals.ametsoc.org/view/journals/clim/31/12/jcli-d-17-0693.1.xml (2018).
54. Mapes, B. E. & Houze, R. A. Cloud clusters and superclusters over the oceanic warm pool. *Mon. Weather Rev*. https://journals.ametsoc.org/view/journals/mwre/121/5/1520-0493_1993_121_1398_ccasot_2_0_co_2.xml (1993).
55. Gray, W. M. & Jacobson, R. W. Diurnal variation of deep cumulus convection. *Mon. Weather Rev*. https://journals.ametsoc.org/view/journals/mwre/105/9/1520-0493_1977_105_1171_dvodcc_2_0_co_2.xml (1977).
56. Yang, G.-Y. & Slingo, J. The diurnal cycle in the tropics. *Mon. Weather Rev.* **129**, 784–801 (2001).
57. Atlas, R. L., Bretherton, C. S., Sokol, A. B., Blossey, P. N. & Khairoutdinov, M. F. Tropical cirrus are highly sensitive to ice microphysics within a nudged global storm-resolving model. *Geophys. Res. Lett.* **51**, e2023GL105868 (2024).
58. Naumann, A. K., Esch, M. & Stevens, B. How the representation of microphysical processes affects tropical condensate in the global storm-resolving model ICON. *Atmos. Chem. Phys.* **25**, 6429–6444 (2025).
59. Ohno, T., Noda, A. T. & Satoh, M. Impacts of sub-grid ice cloud physics in a turbulence scheme on high clouds and their response to global warming. *J. Meteorol. Soc. Jpn. Ser. II* **98**, 1069–1081 (2020).
60. Haslehner, K., Gasparini, B. & Voigt, A. Radiative heating of high-level clouds and its impacts on climate. *J. Geophys. Res. Atmos.* **129**, e2024JD040850 (2024).
61. Deutloff, J. Data to accompany Facets of the Tropical High-Cloud Feedback in a Global Storm-Resolving Model by Deutloff et al., 2026 [Data set]. *Zenodo*. https://doi.org/10.5281/zenodo.20445604 (2026).
62. Deutloff, J. Code to accompany Facets of the Tropical High-Cloud Feedback in a Global Storm-Resolving Model by Deutloff et al., 2026 (1.2). *Zenodo.* https://doi.org/10.5281/zenodo.20445583 (2026).

## Acknowledgements

The authors thank Blaž Gasparini, Seth Seidel, Sandrine Bony, Mark Zelinka, Martin Singh and James Ruppert for inspiring discussions and Lukas Kluft and Sebastian Rast for assisting with the ICON simulations. This research was funded by the Deutsche Forschungsgemeinschaft (DFG, German Research Foundation) under Germany's Excellence Strategy—EXC 2037 "CLICCS—Climate, Climatic Change, and Society"—Project Number: 390683824, contribution to the Earth and Society Research Hub (ESRAH) of the University of Hamburg. This work used resources of the Deutsches Klimarechenzentrum (DKRZ) granted by its Scientific Steering Committee (WLA) under project ID bm1183. The publication fees were covered by the Open Access Publication Fund of the University of Hamburg.

## Author contributions

J.D., S.A.B., J.W., and A.K.N. contributed to designing the research. J.D. carried out the research and wrote the paper with input from all co-authors. All authors have read and approved the manuscript.

## Funding

Open Access funding enabled and organized by Projekt DEAL.

## Competing interests
The authors declare no competing interests.

## Additional information
**Supplementary information** The online version contains supplementary material available at https://doi.org/10.1038/s41612-026-01463-z.

**Correspondence** and requests for materials should be addressed to Jakob Deutloff.

**Reprints and permissions information** is available at http://www.nature.com/reprints

**Publisher's note** Springer Nature remains neutral with regard to jurisdictional claims in published maps and institutional affiliations.

**Open Access** This article is licensed under a Creative Commons Attribution 4.0 International License, which permits use, sharing, adaptation, distribution and reproduction in any medium or format, as long as you give appropriate credit to the original author(s) and the source, provide a link to the Creative Commons licence, and indicate if changes were made. The images or other third party material in this article are included in the article's Creative Commons licence, unless indicated otherwise in a credit line to the material. If material is not included in the article's Creative Commons licence and your intended use is not permitted by statutory regulation or exceeds the permitted use, you will need to obtain permission directly from the copyright holder. To view a copy of this licence, visit http://creativecommons.org/licenses/by/4.0/.

© The Author(s) 2026